Accelerated endothelial wound healing on microstructured substrates under flow

Franco, Davide ; Milde, Florian ; Klingauf, Mirko ; Orsenigo, Fabrizio ; Dejana, Elisabetta ; Poulakikos, Dimos ; Cecchini, Marco ; Koumoutsakos, Petros ; Ferrari, Aldo ; Kurtcuoglu, Vartan

DOI: https://doi.org/10.1016/j.biomaterials.2012.10.007

Accelerated endothelial wound healing on microstructured substrates under flow

*Davide Franco[a], Florian Milde[c], Mirko Klingauf[a,b], Fabrizio Orsenigo[d], Elisabetta Dejana[d], Dimos Poulikakos[a], Marco Cecchini[b], Petros Koumoutsakos[c], Aldo Ferrari[a, †, *] and Vartan Kurtcuoglu[e,†]*

a. Laboratory of Thermodynamics in Emerging Technologies, Department of Mechanical and Process Engineering, ETH Zurich, Sonneggstrasse 3, CH-8092 Zurich, Switzerland;
b. NEST, Istituto Nanoscienze-CNR, Piazza San Silvestro 12, I-56126 Pisa, Italy;
c. Chair of Computational Science, ETH Zurich, Universitätstrasse 6, CH-8092, Switzerland;
d. FIRC Institute of Molecular Oncology, Via Adamello 16, I-20139 Milan, Italy and Department of Biosciences, School of Sciences, Milan University, Milan
e. The Interface Group, Institute of Physiology, University of Zurich, Winterthurerstrasse 190, CH-8057, Switzerland

†. Equal contribution

[*] To whom correspondence should be addressed.

Dr. Aldo Ferrari
ETH Zurich
Laboratory of Thermodynamics in Emerging Technologies
Sonneggstrasse 3, ML J 27.1
CH-8092 Zurich
SWITZERLAND
Phone: +41 44 632 25 88
Fax: +41 44 632 11 76
aferrari@ ethz.ch, dpoulikakos@ethz.ch

1. INTRODUCTION

The vascular endothelium regulates the transport of substances from the blood into the vessel wall [1-2]. Disturbance of this regulatory function, resulting for example from endothelial injury, can cause cardiovascular disease [3]. Understanding and expediting the healing of the endothelium after wounding is thus necessary to avoid focal disease onset.

Cell-to-cell adhesion within a monolayer of endothelial cells (ECs) is ensured by tight junctions and adherens junctions. These are specialized biological structures through which the cohesion of the endothelium is maintained [4]. However, a differentiated endothelium is far from a static sheet of connected cells: Constitutive planar cell movements effect a continuous and dynamic remodeling of the cell junctions [2, 5-6].

The migratory potential of ECs and their mechanical interconnection are fundamental factors in the response of a monolayer when its continuity is compromised by a wound [5-6]. ECs react to the open space by polarizing and migrating into the wound area collectively, i.e. under maintenance of cell-to-cell adhesions [7], to reestablish a confluent monolayer [5-6, 8-12]. This process relies on a modular control of a number of cellular activities to (i) induce directed migration of the cells at the wound interface (border cells), (ii) modulate the autonomous random migration of the inner cells, and (iii) coordinate cell motion within the endothelium [5-6]. Eventually, this response orients sheet migration toward the wound while preserving monolayer connectivity [6].

The current knowledge on wound healing derives from *in vitro* experiments with monolayers moving on flat substrates [6, 9, 12]. Yet *in vivo,* ECs interact with a topographically complex basal matrix [13]. The effect of topographical features with size and orientation similar to those presented by the extracellular matrix has been analyzed previously using substrates engineered by

means of nanoimprint lithography [14-15]. These studies demonstrated that surface texture affects migration and polarization of individual ECs substantially [16-17]. Contact guidance is responsible for these effects. This process is based on the physical confinement of transmembrane receptors of the integrin family, which controls biological contact between the cell and its substrate through the establishment and maturation of focal adhesions [15, 18]. Less attention has been paid so far to the influence of topography on entire monolayers as opposed to individual cells [19].

Adherens Junctions (AJs) play a pivotal role in the collective migration of ECs [7, 20]. Vascular Endothelial Cadherin (VEC), a member of the cadherin transmembrane protein family localized at AJs of ECs, is necessary for the mechanical cohesion of cells in the monolayer. When VEC is down-regulated *in vitro*, border cells still enter the wound, but lose connection to the inner cell lines [6]. Conversely, when cell-to-cell adhesion is strongly reinforced, directed migration of border cells is hampered and wound closure slows down [5]. Fine modulation of the mechanical linkage between ECs within the range of the above mentioned two extremes appears, therefore, to be critical in facilitating migration toward the wound while maintaining monolayer integrity [7, 12]. Factors that influence the stability of AJs are thus likely to affect endothelial wound healing [7]. Among these, flow-mediated endothelial Wall Shear Stress (WSS) and substrate topography are known to play a critical role in the control of vascular permeability *in vivo*. Previous studies reported on the combined effect of substrate topography and flow either on single cell migration or on the morphology of confluent monolayers [21-22]. However, their combined contribution to wound healing, although likely to be important, has never been addressed.

We recently demonstrated that the dynamic state of AJs in the endothelium is regulated through the phosphorylation of VEC [23]. WSS values up to 1.4 Pa activate junctional Src, both *in vivo*

and *in vitro*, thus rendering VEC responsive to a number of inflammatory stimuli. In particular, tyrosine phosphorylated-VEC (pY-VEC) can be quickly withdrawn from AJs to induce a transient reduction of the adhesion strength, which increases vascular permeability [23].

Here we investigate the interplay between substrate topography and flow-mediated WSS during wound healing of entire endothelial monolayers. Endothelial monolayers were grown on topographically modified substrates and exposed to controlled levels of WSS within a custom designed parallel plate flow chamber. We recorded and analyzed the wound healing dynamics under variable configurations defined by the relative orientations of the wound, topography, and flow.

2. MATERIAL AND METHODS

2.1 Substrate fabrication

Gratings with depth, line width, and pitch of 1 μm were imprinted on 180 μm thick untreated cyclic olefin copolymer (COC) foils (Ibidi, Germany) using nanoimprint lithography (NIL) as previously reported [15, 16]. At the end of the fabrication procedure, the substrates were treated with oxygen plasma (100 W for 30 seconds) to increase the hydrophilicity of the surface and to promote cell adhesion.

2.2 Antibodies

The following primary antibodies were used: Mouse anti-vinculin (V4505) purchased from Sigma Aldrich (USA), goat anti-VEC (Vascular Endothelial Cadherin; #6458) from Santa Cruz Biotechnology Inc. (USA) and rabbit pY658-VEC [23]. The secondary antibodies applied were: goat anti-rabbit HRP (#65-6120), donkey anti-goat-alexa-488 (A11055) and donkey anti-mouse-alexa-488 (A21202), all from Invitrogen (USA).

2.3 Cell Culture

Human umbilical vein endothelial cells (HUVEC; Invitrogen, USA) were grown in medium 200PRF supplemented with fetal bovine serum 2% v/v, hydrocortisone 1 μg/ml, human epidermal growth factor 10 ng/ml, basic fibroblast growth factor 3 ng/ml and heparin 10 μg/ml (all reagents from Invitrogen) and were maintained at 37°C and 5% CO_2. All reported experiments were performed using cells with less than seven passages *in vitro*. The substrates were sterilized by overnight treatment with ethanol and rinsed three times with PBS before starting the coating procedure. The substrates were then coated with gelatin according to the

protocol by Lampugnani et al. [24]. The substrates were stored at 4°C until the seeding of the cells. To generate a confluent monolayer, cells were seeded on COC substrates at high density ($3.5\text{-}5x10^4$ cell/cm^2) and cultured for three days.

2.4 Wound healing experiments

A custom designed parallel plate flow chamber was used to apply a constant shear stress to the monolayers during wound healing (Figure 1). The shear stress applied on the cells (τ) can be expressed as function of the channel dimensions (width, w and height, h), medium properties (viscosity, μ) and volumetric flow rate (Q) using the calculation for wall shear stress in a rectangular channel: $\tau=6Q\ \mu/wh^2$ [23]. While channel dimensions and medium properties were fixed in our experimental setup (w=20 mm, h=0.3 mm, $\mu=8.4*10^{-4}$ Pa*s) , the flow rate was controlled using a peristaltic roller pump (Model 66, Harvard Apparatus) to apply WSS of 1.4 Pa to the endothelial cell monolayer. A compliance element was inserted between the roller pump and the flow chamber to dampen flow pulsation.

Before starting the wound healing experiments, cells were labeled using a DiD Vybrant solution (Invitrogen). The cell monolayer was incubated for 40 minutes at 37°C with 1 ml of normal growth medium supplemented with 3 µl of the labeling dye. The staining solution was then substituted with fresh growth medium and the samples were kept at 37°C and 5% CO_2 for 15 minutes before wounding. A longitudinal wound was mechanically implemented with a pipette tip as described in [25]. Scanning electron microscopy images were acquired to demonstrate that the substrate is not damaged upon wounding the endothelial monolayer (Supplementary Figure 1). Depending on the dimension of the pipette tip, small (200 µm<width<350 µm) or large (500 µm<width<700 µm) wounds were reproducibly generated. In particular, wounds were always

oriented perpendicular to the direction of gratings. After wounding of the monolayer, the substrate was placed in the flow chamber and a constant WSS of 1.4 Pa was applied to the cells.

For the Src inhibition experiments, the specific inhibitor PP1 (Enzo Life Sciences Inc., USA) was added to the culture media at a final concentration of 10 μM as reported in [23]. The monolayer was then incubated at 37°C and 5% CO_2 for 30 minutes and afterwards the wound was mechanically implemented before placing the substrate into the flow chamber. The medium flowing in the flow chamber was also supplemented with PP1 at the same concentration to sustain the Src inhibition during the entire wound healing experiment.

2.5 Immunostaining

HUVECs were fixed and permeabilized for 3 minutes with 3% paraformaldehyde (PFA) and 0.5% Triton-X100 in PBS at room temperature (RT). The cells were then post-fixed with 3% PFA in PBS for 15 minutes. After washing the samples three times for 5 minutes with PBS, they were incubated with 5% bovine serum albumin (BSA) and 5% donkey serum in PBS for 1 hour at RT. The samples were incubated either with anti-vinculin primary antibody together with TRITC-phalloidin (Sigma, USA) or with anti-VEC together with anti-pY658-VEC primary antibodies overnight at 4°C. Subsequently, the samples were rinsed four times for 1 hour with 5% BSA in PBS and then were incubated with anti-mouse-alexa-488 secondary antibody and goat anti-rabbit HRP together with anti-goat-alexa-488 secondary antibodies for 45 minutes at RT. Finally, the samples were washed three times (1 hour each) in PBS, post-fixed for 2 minutes in 3% PFA, briefly washed again with PBS, mounted with DAPI-containing Vectashield (Vector Labs Inc., USA) and immediately imaged.

2.6 Video acquisition

Live wound healing was imaged using an inverted Nikon-Ti wide-field microscope (Nikon, Japan) equipped with an Orca R-2 CCD camera (Hamamatsu Photonics, Japan) and an incubated chamber (Life Imaging Services, Switzerland). Both the flow chamber and the medium reservoir were maintained at a controlled temperature of 37°C and CO_2 concentration of 5%. Images were collected with a 20X, 0.45 NA long-distance objective (Plan Fluor, Nikon, Japan). The experiment was started to automatically collect images in the TRITC channel with a time resolution of 15 minutes for a total of 16 hours. Using the large image function (NIS Elements, Nikon, Japan), a field of 3 by 3 single images was acquired for each set position. Focal drift during the experiments was eliminated using the scope's PFS autofocus system. At the end of the experiment, the resulting time-lapses of each set position were converted into individual 16 bit movies for analysis.

Fluorescent image stacks of HUVEC immunostained for VEC and pY658-VEC were acquired with a 60X, 1.2 NA water immersion objective (PlanApo, Nikon) using a FITC and a TRITC filter, respectively.

Confocal images of immunostained HUVECs were collected with a Leica SP2-AOBS (Leica, Germany) microscope using a 63X, 1.4 NA, oil immersion objective (Plan-Apo, Leica, Germany). DAPI emission was excited with the 405 nm wavelength of a solid-state laser and collected in the 410-480 nm optical window. Vinculin signal was acquired exciting the Alexa-488 emission with the 488 nm wavelength of an Argon laser and collected in the 500-550 nm optical window. F-actin was imaged by exciting the TRITC-phalloidin emission with the 561 nm wavelength of a solid-state laser and collecting the signals in the 575-675 nm optical window.

2.7 *Video analysis*

The cell density and the individual cell-substrate contact area were measured using ImageJ (National Institutes of Health, USA). In particular, the cell density was measured using the "Cell Counter" tool, while the area of cells in contact with the substrate was obtain using first the "Freehand selection" and then the "Measurements" tools. Cell orientation was measured analyzing the TRITC-phalloidin stained images with the "Directionality" tool of Fiji (National Institutes of Health, USA). The obtained value in degrees was normalized relative to the flow direction. The range of possible alignment angles between cells and flow is 0° to 90°. Thus a value close to 0° indicates perfect alignment while a value of 45° indicates no alignment.

Quantitative analysis of wound healing was performed using the Cell Image Velocimetry (CIV) Matlab toolbox [26]. Reported values are mean values over the first 7.5h (30 frames) of the experiment, considering cells inside a region extending 250 μm into the cell layer. The velocity field provided by the CIV analysis is quantified by the mean cell layer speed (mean velocity magnitude), directed migration (mean velocity projection in the axis aligned perpendicular to the initial wound orientation) and the angular velocity distribution, a measure for the effective migration contribution along 32 equally spaced angular sectors (i.e. with angular bin size of 360°/32).

The relative edge protrusion was obtained using first the "Freehand line" and then the "Measurements" tools of ImageJ. The edge length measured at different time steps was normalized by the edge length measured at the beginning of the experiment (t=0). A value above unity indicates that the edge length increases due to the formation of cell protrusions, while a value below unity indicates that the edge length decreases due to a straightening of the edge profile.

The Pearson's coefficient was extracted from each image stack using the colocalization section of Imaris (Bitplane, Switzerland). During the colocalization analysis, threshold values calculated based on [27] were imposed for both the green and the red channels.

Focal adhesion size was measured using confocal images of HUVECs stained with anti-vinculin antibody. First the images were loaded in ImageJ, transformed to binary images using the automatic threshold function and then analyzed with the "Analyze Particle" tool. The lower and upper limits for FA size were set to 0.6 μm^2 and 5 μm^2, respectively.

2.8 Statistical analysis

All statistical comparisons were performed using a non-parametric Mann–Whitney (α=0.05) or a Kolmogorov-Smirnov test. All quantitative measurements reported are expressed as average values ± the standard error of the mean. The total number of events counted is always indicated in the presented graphs.

3. RESULTS

3.1 Experimental configurations

To quantify the contribution of substrate topography to the dynamics of wound healing in a flow environment, endothelial monolayers were grown on control flat substrates as well as on gratings. In the latter case, the size and periodicity of topographical features was chosen to maximize contact guidance [16].

The investigated experimental configurations were defined by the relative orientation of topography, wound and flow. We generated longitudinal small (200 μm<width<350 μm) or large (500 μm<width<700 μm) wounds, which on textured substrates were oriented perpendicular to the gratings. Substrates were positioned in the flow chamber so as to have wounds aligned either parallel or perpendicular to the direction of flow. Importantly, the latter configuration is accompanied by an asymmetry between the upstream and downstream edges of the cell monolayer bordering the wound with respect to the flow. We define as upstream edge the cell edge closer to the inlet of the flow chamber (Figure 1).

3.2 Effect of substrate topography and WSS on endothelial monolayers

Differentiated endothelia are characterized by the monolayer density and polarization [5-6, 24]. Figure 2a reports the cell density measured in confluent, growth-arrested monolayers on flat substrates or gratings. Under static conditions the cell density was significantly higher on flat (1025±48 cells/mm^2) than on textured (870±58 cells/mm^2) substrates. When confluent monolayers grown on flat substrates were exposed to WSS, the cell density was reduced (875±46 cells/mm^2) while flow conditioning had no significant effect on gratings (782±74 cells/mm^2).

The area of ECs grown on flat substrates under static conditions was on the average 902±73 μm^2 (Figure 2b) and the cells were randomly oriented within the monolayer (Figure 2c). Exposure to WSS significantly enhanced cell spreading on flat substrates (average cell area = 1130±148 μm^2; Figure 2b) and improved cell orientation toward the direction of flow (average orientation 34±4°; Figure 2c). Substrate topography had a similar effect on EC spreading (average cell area = 1068±103 μm^2; Figure 2b), but a significantly stronger effect on the monolayer polarity. Here, cells aligned within 17±4° to the direction of the gratings (Figure 2c). The combination of aligned substrate topography and WSS did not further improve cell spreading or polarization (Figure 2).

Altogether, these results demonstrate that the effects of substrate topography and WSS were similar and resulted from the enhanced spreading of individual ECs in the monolayers. Importantly, when the two stimuli were applied together, the density never dropped below the threshold value of ~800 cells/mm^2; thus suggesting that a minimal cell density is necessary to ensure monolayer integrity.

The distribution of microfilaments and vinculin in the monolayers confirmed a better alignment of cells interacting with gratings (Figure 2d). Interestingly, the size of focal adhesions was visibly increased on gratings and in the presence of flow (Supplementary Figure 2a), indicating a stronger adhesion to the substrate [16]. The alignment of the actin cytoskeleton and of focal adhesions confirms the results of cell polarization (Figure 2d and Supplementary Figure 2b): EC polarization in the monolayer was induced both by gratings and by flow.

3.3 Effect of topography on wound healing under flow

Healing of longitudinal wounds oriented perpendicularly to the flow proceeded slowly on flat substrates (Figure 3a). For large wounds, 15 hours after wounding a significant portion of the

originally open space remained uncovered. Healing was accelerated on gratings (Figure 3b). In particular, in the case of large wounds (Figure 3b), the upstream and downstream edges converged already at 8 hours after wounding, and a *bona fide* confluent monolayer was reestablished after 15 hours (Supplementary Movie 01).

In-depth analysis of wound healing dynamics revealed that two effects combine to promote wound coverage on gratings: (i) the enhancement of counterflow migration from the downstream edge and (ii) the increased range of migration towards the open space. The migration range is defined as the time integral of wound edge speed from wounding to a halt in edge migration. It is thus an indicator for the maximum coverable wound size.

During the first hours of wound healing on flat substrates, the angular distribution of cell motion shows that the cell velocity components in the wound closure direction were significantly reduced for cells located at the downstream edge (Figure 3c). These cells advanced with low speed (0.09±0.01 μm/min) toward the open space. Additionally, a significant component of retrograde motion was present. Cells located at the upstream edge migrated toward the open space with higher speed (0.18±0.01 μm/min) and only minimal retrograde motion was detected. This migration asymmetry was remarkably absent on gratings. Here, the two fronts advanced toward the open space with comparable speeds (upstream 0.19±0.02 μm/min; downstream 0.18±0.01 μm/min) and at both edges the retrograde motion was not significant (Figure 3c). The overall impact on directed migration (i.e. cell migration in the wound closing direction) for both flat and gratings substrates is summarized in Figure 3d. When wounds were oriented parallel to the flow (and still perpendicular to the gratings), migration directed toward the open space proceeded from both edges with comparable speed independent of substrate topography (Supplementary Figure 3). Thus, the effect of flow on the speed of directed migration was only

present in the case of counterflow migration. Summarizing, these data demonstrate that cell motion on a flat substrate against the flow is severely hampered, thus limiting the contribution of cells at the downstream edge to the process wound healing. The presence of gratings is sufficient to reestablish directed migration from both edges.

The range of migration toward the open space was also enhanced by gratings. On flat substrates, the speed of directed migration decreased over time (Supplementary Figure 4) and the advancement of the two cell edges eventually stopped (Figure 3a), leaving the wound open. In general, on flat substrates, wound closure was partial and limited to 165±33 μm from the upstream edge and to 72±28 μm from the downstream edge (Figure 3e). In the presence of gratings, there was no reduction in the speed of wound edge movement over time, enabling the closure of large wounds (Figure 3e and Supplementary Figure 4). These results demonstrate that flow reduces the range of directed migration [9], thereby limiting the wound closure potential on flat substrates. Contact with the gratings was sufficient to increase the migration range, resulting in complete closure of large wounds.

3.4 Individual vs. collective cell migration during wound healing

During wound healing under static conditions, cells at the wound edge migrate directionally into the open space. Propagation of the directed motility signal into the cell monolayer depends on the strength of cell-to-cell adhesions between the border and the inner cells [5]. In order to understand the different responses observed on flat and gratings substrates during wound healing under flow (Figure 3), we analyzed the behavior of cells at the upstream and downstream wound edges.

A magnified view of the downstream edge (Figure 4a) in the early phases of wound healing (first 2 hours) shows the evolution of the cell boundary. On flat substrates, intrusions of border cells into the open space were short lived, and a straight boundary was maintained over time (Figure 4a). On gratings, pioneer cells entered the wound and generated stable fingerings that led the migration. This effect was quantified measuring the relative edge protrusions produced at the downstream edge during the early phases of wound healing (Figure 4c). This observation suggests that flow affects directed migration from the downstream edge by hindering the spreading of border cells into the wound. Gratings counteract this effect by stabilizing the protrusions of border cells, thus promoting directed migration.

Cells at the upstream edge migrated into the open space along the flow (Figure 4b). On flat substrates, border cells moved toward the wound area, but directed migration was not propagated to the inner cells. During the process of healing large wounds, this loss of cohesion led to individual cell migration (Figure 4b). It is noteworthy that individually migrating cells were removed by the flow and did not contribute to healing (Supplementary Movie 02). On gratings, cells from the two edges migrated collectively into the wound and individual cell migration was never detected (Figure 4d). This behavior is reflected by the measurement of the angular correlation between the motility of border and inner cells (Figure 4d).

These results suggest that flow leads to loss of cell-to-cell contact between border and inner cells, thereby promoting individual cell migration into the wound. Surface topography counteracts this effect, promoting collective migration under flow.

3.5 VEC phosphorylation is inhibited by topography

To demonstrate that topography reinforces the mechanical linkage between ECs in the monolayer, we investigated the stability of AJs by analyzing VEC phosphorylation levels. WSS increases the basal levels of VEC phosphorylation on flat substrates as revealed by a specific antibody directed to a phospho-peptide of the cytoplasmic region of VEC (pY658-VEC) [23]. Wounding also triggers phosphorylation of VEC at the junctions between border and inner cells [24].

Figure 5a shows the levels of pY658-VEC detected in cell monolayers on flat substrates and gratings under both static and flow conditions. Co-localization with total VEC demonstrates that gratings significantly reduced the basal levels of pY658-VEC at static conditions and counteracted the effect of WSS (Figure 5b). On flat substrates one hour after wounding, we consistently detected increased levels of pY685-VEC at the junctions between border and inner cells (Figure 5c). This effect was not observed on gratings where the wound edges showed low levels of VEC phosphorylation (Figure 5c).

Based on this, we conclude that substrate topography inhibits the phosphorylation of VEC induced by WSS or by the implementation of a wound. The data further indicate that the basal interaction with gratings is sufficient to stabilize the mechanical connection between ECs in the monolayer.

3.6 Src inhibition promotes wound healing under flow

Tyrosine phosphorylation of VEC is mediated by junctional Src [20, 23]. In order to test the hypothesis that an increased stability of AJs at the wound edges is sufficient to promote collective

migration under flow and thus the healing of large wounds, we performed a set of wound healing experiments in the presence of a specific Src inhibitor (Figure 6).

In treated monolayers grown on flat substrates, large wounds healed quickly (Figure 6a). In particular, Src inhibition promoted collective cell motion. Additionally, it increased the speed of counterflow migration from the downstream edge (Figures 6b and c) and the range of directed migration from both edges (Figure 6d) to levels comparable to those measured on gratings (Figures 6c and d). These results demonstrate that the stabilization of AJs at the wound edges is sufficient to ensure the cohesion between border and inner cells, thus enabling the healing of large wounds under flow.

4. DISCUSSION

A modulation of the mechanical linkage between cells in a monolayer is essential for expedient wound healing by directed migration while preserving the sheet integrity [5, 26]. Here, we demonstrated that flow-mediated wall shear stress and substrate topography cooperate to enable a dynamic control of cell-to-cell contact stability upon healing. Prior investigations of the interplay between basal and lateral proteins on structured substrates revealed the presence of a bidirectional communication controlling the direction and the degree of cell migration [28]. Our results indicate a further level of control by which the basal interaction with substrate topography demotes the flow-induced phosphorylation of vascular endothelial cadherin and thereby sets the stability of lateral connections between cells to an optimal intermediate value (Figure 6).

On flat substrates, wall shear stress reduces the strength of cell-to-cell adhesions and contributes to the loss of monolayer integrity upon wound healing (Figure 4). In this way, the presence of flow induces a switch from collective to individual cell migration, and compromises the relay from border to inner cells. Individual cell migration is not beneficial for wound healing under flow, as isolated cells fail to resist shear stress and are flushed away (Figure 3). As a result, the open space simply moves to inner positions, creating a new wound edge. The process is reiterated to the point that directed migration eventually stops, and the monolayer integrity is compromised (Figure 3 and Supplementary Figure 4). Consequently, endothelial monolayers grown on flat substrates have a limited healing potential (Figure 3).

On topographically-modified substrates, the maintenance of lateral cohesion has a beneficial effect: It allows for the transmission of directed motility from border to inner cells, thereby preventing individual cell migration (Figure 4). This, in turn, enhances the range of directed cell migration and augments the wound closing potential of the endothelial sheet. When the activity

of Src is pharmacologically inhibited, this effect is replicated on flat substrates (Figure 6), which indicates that substrate topography promotes wound healing through the control of adherence junction stability.

In wounds that are oriented perpendicular to the flow, cells at the downstream edge must polarize and move against the flow. As a result, on a flat substrate, these cells struggle to produce stable membrane protrusions into the open space (Figure 4). They migrate with low speed into the wound, and the typical cell fingerings that lead the way to healing are demoted (Figure 4). Topographic modifications of the substrate strongly influence spreading and polarization of individual endothelial cells [16]. Such textures also affect entire endothelial monolayers, yielding (i) increased cell polarization and spreading (Figure 2) and (ii) reinforced integrin contacts, thus generating adhesions that are significantly more mature (Figure 2 and Supplementary Figure 2). When border cells migrate into the wound, the stabilization of actin-based membrane protrusions may benefit from the effect of gratings on integrin contacts. The combination of stronger adhesion to the substrate and enhanced cell polarization will allow border cells to resist the opposing flow and thus support directed migration.

5. CONCLUSIONS

We developed a specialized bioreactor to study endothelial wound healing in a physiological flow environment. The effect of wall shear stress (WSS) on cell monolayers was analyzed as a function of the basal substrate. Flat surfaces were compared to topographically rich substrates, generated by means of nanoimprint lithography, mimicking the features of a basal matrix. These experiments revealed a complex regulation of cell motility yielding effective wound closure only when the contact with topography contributed to the modulation of the cell-to-cell junction stability. We demonstrate a pivotal role of Vascular Endothelia Cadherin (VEC) in this regulation. Its Src-dependent phosphorylation is promoted by flow-mediated WSS and by the wounding while is counteracted by the interaction with the basal topography. The importance of this result is twofold. First it defines a model environment to study cell behavior upon wound healing. Second, it opens the way to strategies aimed at improving the performance of biomedical implants through surface modifications.

Figures

Figure 1. Experimental configuration: Endothelial monolayers are cultured on flat substrates or gratings (left) and a mechanical wound (right) is implemented (**b**). The substrates are then placed inside the flow chamber to have the wound aligned either parallel or perpendicular to flow (**c**). A peristaltic pump is used to apply a constant flow to the cell monolayer (**d**).

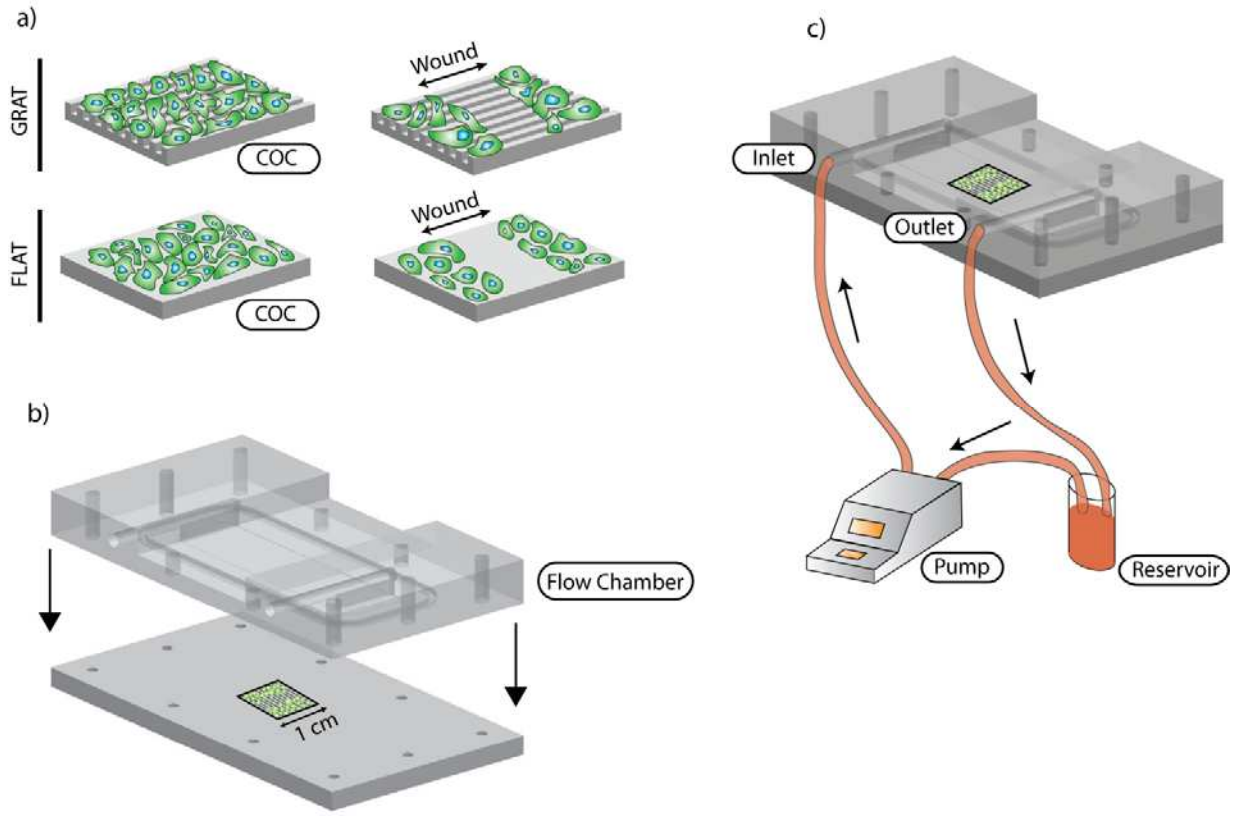

Figure 2. The histograms report the cell density (**a**), the cell area (**b**) and the average alignment (**c**) on flat (FLAT) substrates or gratings (GRAT) with (Flow) or without (Static) flow. The number of analyzed events is reported in the upper right corner. Significant differences between the population means are indicated by asterisks (* for $p<0.05$, ** for $p<0.01$). Error bars represent the measured standard error of the mean. (**d**) Confocal images of immunofluorescent staining showing the distribution of actin filaments (left-red) and vinculin (middle-green) for each experimental condition. The right panels show an overlay of the two channels. The orientation of the gratings is reported in the lower left corner. The blue arrows indicate the direction of the flow. The scale bars correspond to 20 μm.

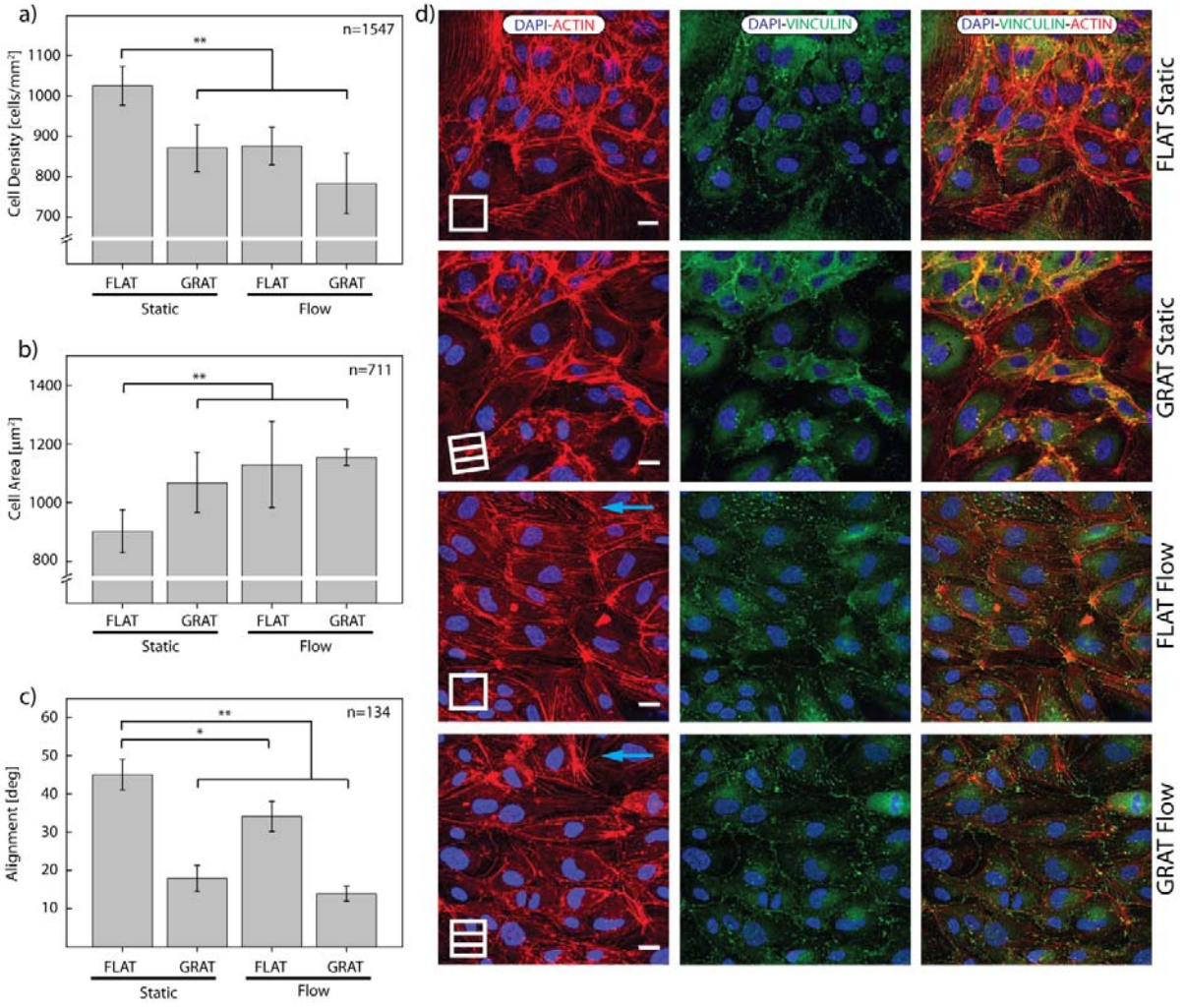

Figure 3. Inverted fluorescent images extracted from a time-lapse of HUVEC wound healing on (**a**) flat substrate and (**b**) on gratings. For both configurations, constant flow (WSS of 1.4 Pa) was applied to the cell monolayer throughout the entire experiment. The blue arrows indicate the direction of the flow. The orientation of the gratings is shown in the first panel (t=0 h) in the center of the wound. The time is reported in the lower right corner of each frame. Scale bar corresponds to 100 μm. (**c**) Angular velocity distributions (in μm/min) of the downstream and upstream edge. The dotted lines represent the standard error of the mean. The plots report the results obtained on flat substrates (FLAT) or on gratings (GRAT). The number of analyzed time-lapses is reported in the lower left corner. The blue arrows indicate the direction of the flow. (**d**) The bar graphs report the velocity of migration in the wound closing direction measured for the two different substrates (FLAT, GRAT). The number of analyzed time-lapses is reported in the upper right corner. Significant differences between the population means are indicated (** for $p<0.01$). Error bars represent the measured standard error of the mean. (**e**) The horizontal bars represent the migration range toward the open space from the upstream and downstream edge measured for the flat substrate (FLAT) and the gratings (GRAT).

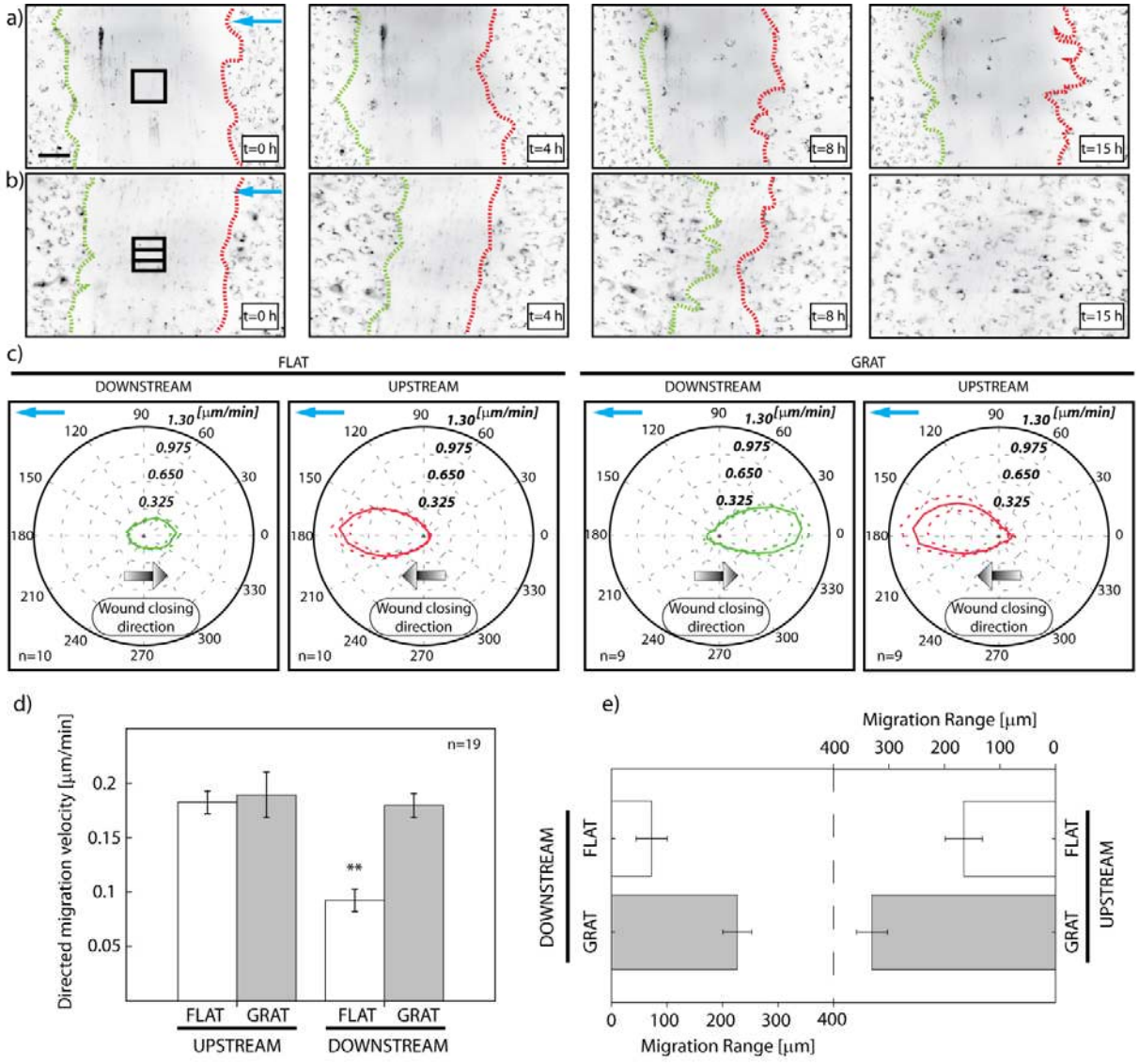

Figure 4. Downstream (**a**) and upstream (**b**) edge migration during wound healing on flat substrates or gratings. The orientation of the gratings is shown in the first panel in the upper left corner. A constant flow (WSS of 1.4 Pa) is applied to the cell monolayer throughout the entire experiment. The blue arrows indicate the direction of the flow. The cell-free area is artificially visualized in red. The time is reported for each frame in the lower right corner. Scale bars correspond to 50 µm. **c)** Relative edge protrusion measured at the downstream edge in the first two hours after wounding. **d)** Angular correlation between border and inner cells at the upstream edge during the first two hours after wounding.

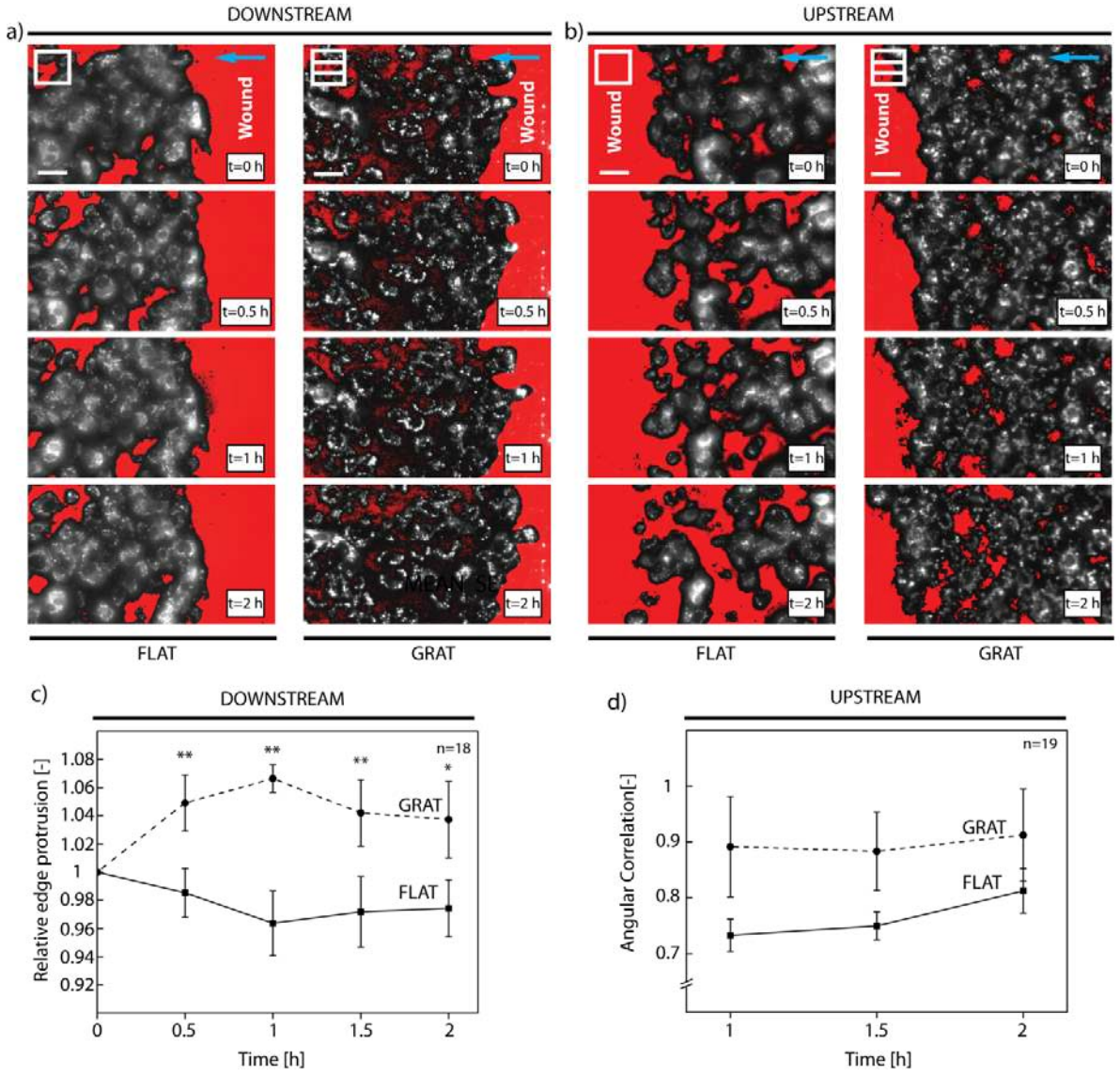

Figure 5. (**a**) Distribution of total VEC (green) and nuclei (blue) are shown in the upper row. Phosphorylated VEC (py-VEC) is depicted in red and shown in the middle row. In the bottom row, the colocalization of the green and the red channels is reported. The orientation of the gratings is shown in the upper left corner. Scale bar corresponds to 20 μm. (**b**) The histograms report the Pearson's correlation coefficient between the green and the red channels on flat (FLAT) or gratings (GRAT) substrates with (Flow) or without (Static) flow. The number of analyzed images is reported in the upper right corner. Significant differences between the population means are indicated (** for $p<0.01$). Error bars represent the measured standard error of the mean. (**c**) Magnified view of the py-VEC and tot-VEC distributions at the wound edge.

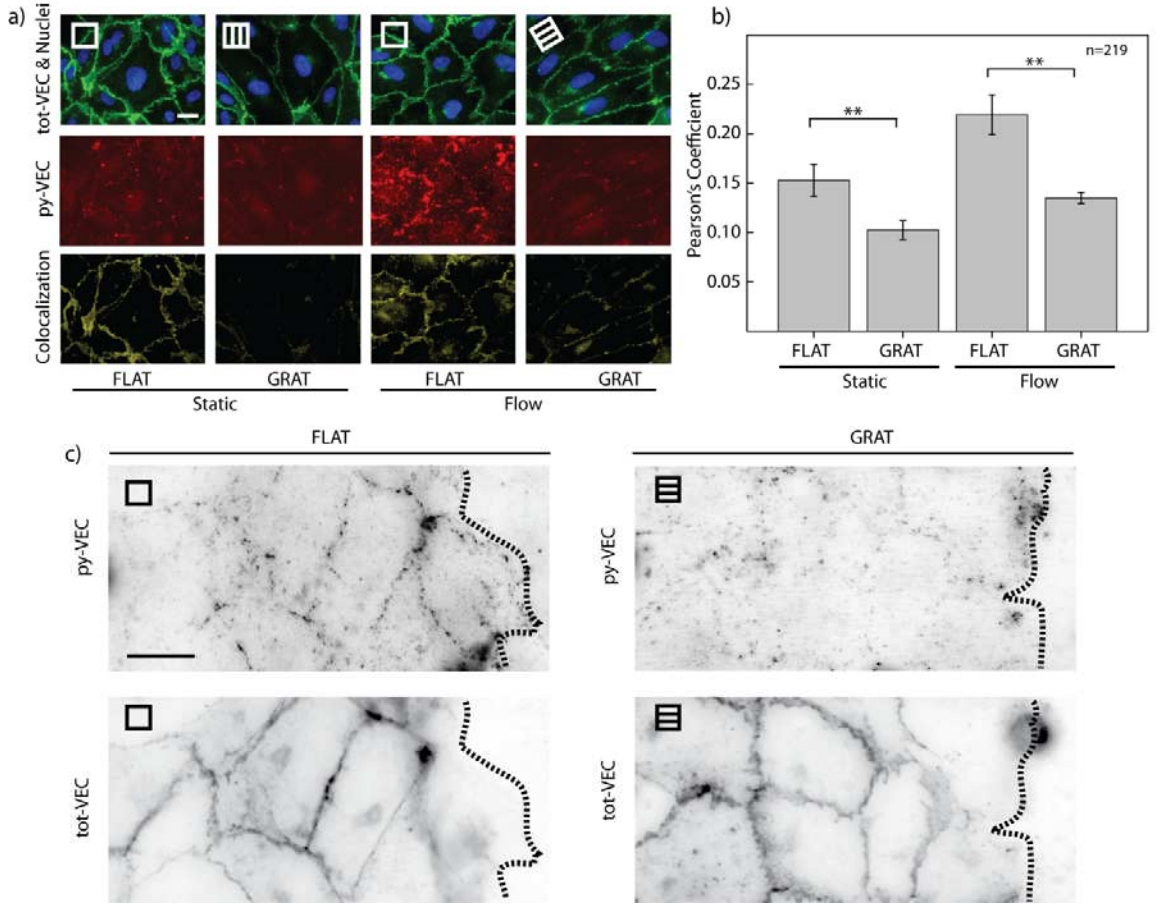

Figure 6. (**a**) Inverted fluorescent images extracted from time-lapse of HUVEC wound healing on flat substrates. A constant flow (WSS of 1.4 Pa) is applied to the cell monolayer throughout the entire experiment. The blue arrows indicate the direction of the flow. The time is reported for each frame in the lower right corner. Scale bar is 100 μm. (**b**) Angular velocity distributions of the downstream and upstream edges. Dotted lines represent the standard error of the mean. The number of analyzed time-lapses is reported in the lower left corner. The blue arrows indicate the direction of the flow. (**c**) The bar graphs report the velocity of directed migration measured for untreated cells on flat substrates (FLAT) or gratings (GRAT) and for PP1-treated cells on flat substrates (FLAT-PP1). The number of analyzed time-lapses is reported in the upper right corner. Significant differences between the population means are reported (* for $p<0.05$, ** for $p<0.01$). Error bars represent the measured standard error of the mean. (**d**) The horizontal bars represent the migration range toward the open space from the upstream and downstream edge measured for untreated cells on flat substrates (FLAT) or gratings (GRAT) and for PP1-treated cells on flat substrates (FLAT-PP1).

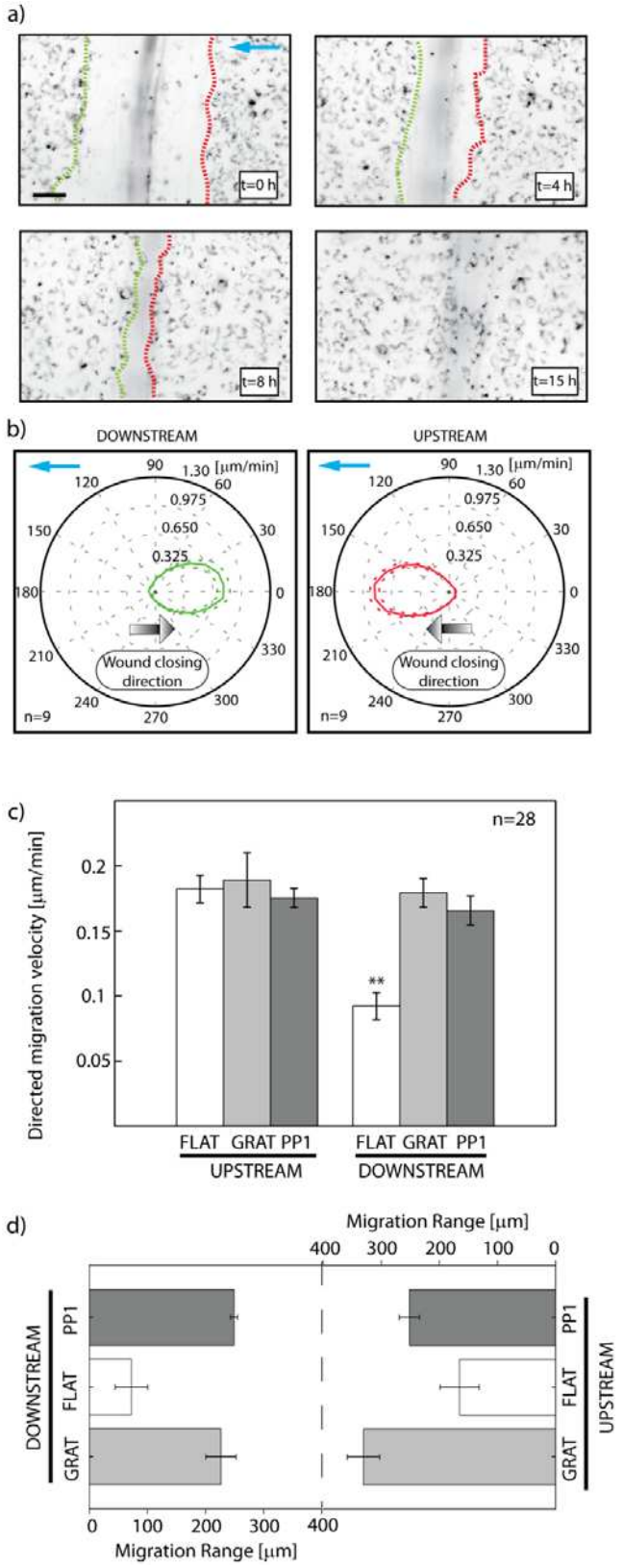
a)
t=0 h
t=4 h
t=8 h
t=15 h
b)
DOWNSTREAM
UPSTREAM
[µm/min]
1.30
0.975
0.650
0.325
Wound closing direction
n=9
c)
n=28
Directed migration velocity [µm/min]
0.2
0.15
0.1
0.05
**
FLAT GRAT PP1
UPSTREAM
FLAT GRAT PP1
DOWNSTREAM
d)
Migration Range [µm]
400 300 200 100 0
DOWNSTREAM
PP1
FLAT
GRAT
UPSTREAM
0 100 200 300 400
Migration Range [µm]

Acknowledgements

This work was supported by the Swiss Federal Innovation Promotion Agency CTI through the EnOp project, as well as by the European Union Seventh Framework Programme (FP7/ 2007-2013) under grant agreement no. NMP4-LA-2009-229289 NanoII and grant agreement no. NMP3-SL-2009-229294 NanoCARD. The research of ED and FO was supported by Associazione Italiana per la Ricerca sul Cancro, European Research Council and European Community Network ANGIOSCAFF-NMP3-LA-2008-214402

References

[1] Dejana E. Endothelial cell-cell junctions: happy together. Nat Rev Mol Cell Biol 2004;5:261-70.

[2] Dejana E, Tournier-Lasserve E, Weinstein BM. The control of vascular integrity by endothelial cell junctions: molecular basis and pathological implications. Dev Cell 2009;16:209-21.

[3] Komatsu R, Ueda M, Naruko T, Kojima A, Becker AE. Neointimal tissue response at sites of coronary stenting in humans: macroscopic, histological, and immunohistochemical analyses. Circulation 1998;98:224-33.

[4] Bazzoni G, Dejana E. Endothelial cell-to-cell junctions: molecular organization and role in vascular homeostasis. Physiol Rev 2004;84:869-901.

[5] Vitorino P, Hammer M, Kim J, Meyer T. A steering model of endothelial sheet migration recapitulates monolayer integrity and directed collective migration. Mol Cell Biol 2011;31:342-50.

[6] Vitorino P, Meyer T. Modular control of endothelial sheet migration. Genes Dev 2008;22:3268-81.

[7] Montell DJ. Morphogenetic cell movements: diversity from modular mechanical properties. Science 2008;322:1502-5.

[8] Petitjean L, Reffay M, Grasland-Mongrain E, Poujade M, Ladoux B, Buguin A, et al. Velocity fields in a collectively migrating epithelium. Biophys J 2010;98:1790-800.

[9] Poujade M, Grasland-Mongrain E, Hertzog A, Jouanneau J, Chavrier P, Ladoux B, et al. Collective migration of an epithelial monolayer in response to a model wound. Proc Natl Acad Sci U S A 2007;104:15988-93.

[10] Szabo A, Unnep R, Mehes E, Twal WO, Argraves WS, Cao Y, et al. Collective cell motion in endothelial monolayers. Phys Biol 2010;7:046007.

[11] Tambe DT, Hardin CC, Angelini TE, Rajendran K, Park CY, Serra-Picamal X, et al. Collective cell guidance by cooperative intercellular forces. Nat Mater 2011;10:469-75.

[12] Trepat X, Fredberg JJ. Plithotaxis and emergent dynamics in collective cellular migration. Trends Cell Biol 2011;21:638-46.

[13] Stupack DG, Cheresh DA. ECM remodeling regulates angiogenesis: endothelial integrins look for new ligands. Sci STKE. 2002;2002:pe7.

[14] Bettinger CJ, Langer R, Borenstein JT. Engineering substrate topography at the micro and nanoscale to control cell function. Angew Chem Int Ed Engl. 2009;48:5406-15.

[15] Ferrari A, Cecchini M, Dhawan A, Micera S, Tonazzini I, Stabile R, et al. Nanotopographic control of neuronal polarity. Nano Lett 2011;11:505-11.

[16] Franco D, Klingauf M, Bednarzik M, Cecchini M, Kurtcuoglu V, Gobrecht J, et al. Control of initial endothelial spreading by topographic activation of focal adhesion kinase. Soft Matter 2011;7:7313-24.

[17] Liliensiek SJ, Wood JA, Yong J, Auerbach R, Nealey PF, Murphy CJ. Modulation of human vascular endothelial cell behaviors by nanotopographic cues. Biomaterials 2010;31:5418-26.

[18] Ferrari A, Cecchini M, Serresi M, Faraci P, Pisignano D, Beltram F. Neuronal polarity selection by topography-induced focal adhesion control. Biomaterials 2010;31:4682-94.

[19] Frohlich EM, Zhang X, Charest JL. The use of controlled surface topography and flow-induced shear stress to influence renal epithelial cell function. Integr Biol (Camb) 2012;4:75-83.

[20] Dejana E, Orsenigo F, Lampugnani MG. The role of adherens junctions and VE-cadherin in the control of vascular permeability. J Cell Sci 2008;121:2115-22.

[21] Morgan JT, Wood JA, Shah NM, Hughbanks ML, Russell P, Barakat AI, et al. Integration of basal topographic cues and apical shear stress in vascular endothelial cells. Biomaterials 2012;33:4126-35.

[22] Uttayarat P, Chen M, Li M, Allen FD, Composto RJ, Lelkes PI. Microtopography and flow modulate the direction of endothelial cell migration. Am J Physiol Heart Circ Physiol 2008;294:H1027-35.

[23] Orsenigo F, Giampietro C, Ferrari A, Corada M, Galaup A, Sigismund S, et al. The constitutive phosphorylation of VE-cadherin in vivo in veins is a priming factor necessary but not sufficient for induction of vascular permeability. Nat Commun 2012.

[24] Lampugnani MG, Corada M, Andriopoulou P, Esser S, Risau W, Dejana E. Cell confluence regulates tyrosine phosphorylation of adherens junction components in endothelial cells. J Cell Sci 1997;110 (Pt 17):2065-77.

[25] Lampugnani MG, Corada M, Caveda L, Breviario F, Ayalon O, Geiger B, et al. The molecular organization of endothelial cell to cell junctions: differential association of plakoglobin, beta-catenin, and alpha-catenin with vascular endothelial cadherin (VE-cadherin). J Cell Biol 1995;129:203-17.

[26] Milde F, Franco D, Ferrari A, Kurtcuoglu V, Poulikakos D, Koumoutsakos P. Cell Image Velocimetry (CIV): boosting the automated quantification of cell migration in wound healing assays. Integr Biol (Camb) 2012. DOI 10.1039/c2ib20113e

[27] Costes SV, Daelemans D, Cho EH, Dobbin Z, Pavlakis G, Lockett S. Automatic and quantitative measurement of protein-protein colocalization in live cells. Biophys J 2004;86:3993-4003.

[28] Borghi N, Lowndes M, Maruthamuthu V, Gardel ML, Nelson WJ. Regulation of cell motile behavior by crosstalk between cadherin- and integrin-mediated adhesions. Proc Natl Acad Sci U S A 2010;107:13324-9.

Supplementary Information

Supplementary Figure 1: Scanning electron microscopy images of the substrates after wounding with pipette tip: (**a**) Wound extending across the gratings (GRAT) and flat (FLAT) substrate. The wound edges are highlighted by a dotted white line. Scale bar is 50 μm (**b**) Detail of wounded region on gratings. There are no apparent damages to the gratings by the pipette tip. Scale bar is 2 μm.

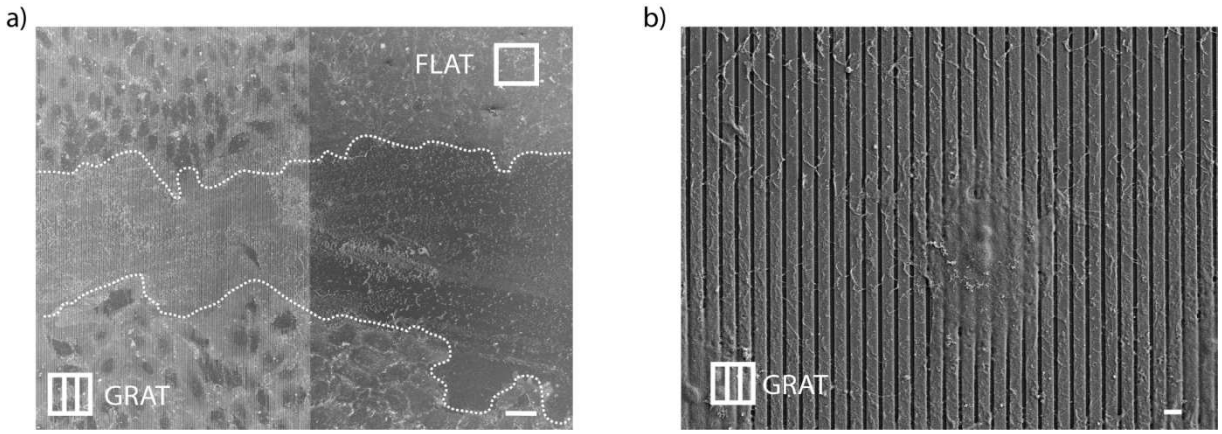

Supplementary Figure 2: Focal adhesion size increases under flow: (**a**) The histograms report the Focal Adhesion (FA) size measured on flat substrates, and on the gratings under static and flow conditions. (**b**) Inverted fluorescent images of HUVECs stained with anti-vinculin antibody for each experimental condition. The blue arrows indicate the direction of the flow. Scale bar is 20 µm.

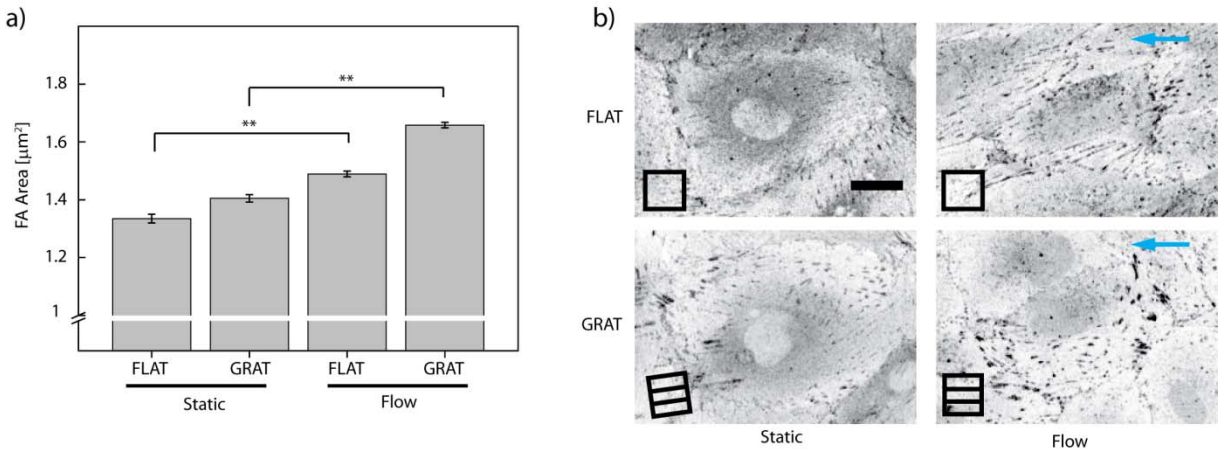

Supplementary Figure 3. HUVECs healing a flow-parallel wound**:** Inverted fluorescent images extracted from a time-lapse of HUVECs wound healing on the (**a-**upper raw-orange) flat substrate and (**a-**lower raw-blu) on grating. For both configurations a constant flow (shear stress of 1.4 Pa) was applied to the cell monolayer throughout the entire experiment. The blue arrows indicate the direction of the flow. The orientation of the gratings is shown in the first panel (t=0 h) in the center of the wound. The time is reported in the lower right corner of each frame. Scale bar corresponds to 100 µm. (**b**) Angular velocity distributions measured both on the flat substrate (FLAT) and on the grating (GRAT). The dotted lines represent the standard error of the mean. The number of analyzed time-lapses is reported in the lower left corner. The blue arrows indicate the direction of the flow. (**c**) The histograms report the directed migration velocity for the two different substrates (FLAT, GRAT). The number of analyzed time-lapses is reported in the upper left corner. Error bars represent the measured standard error of the mean.

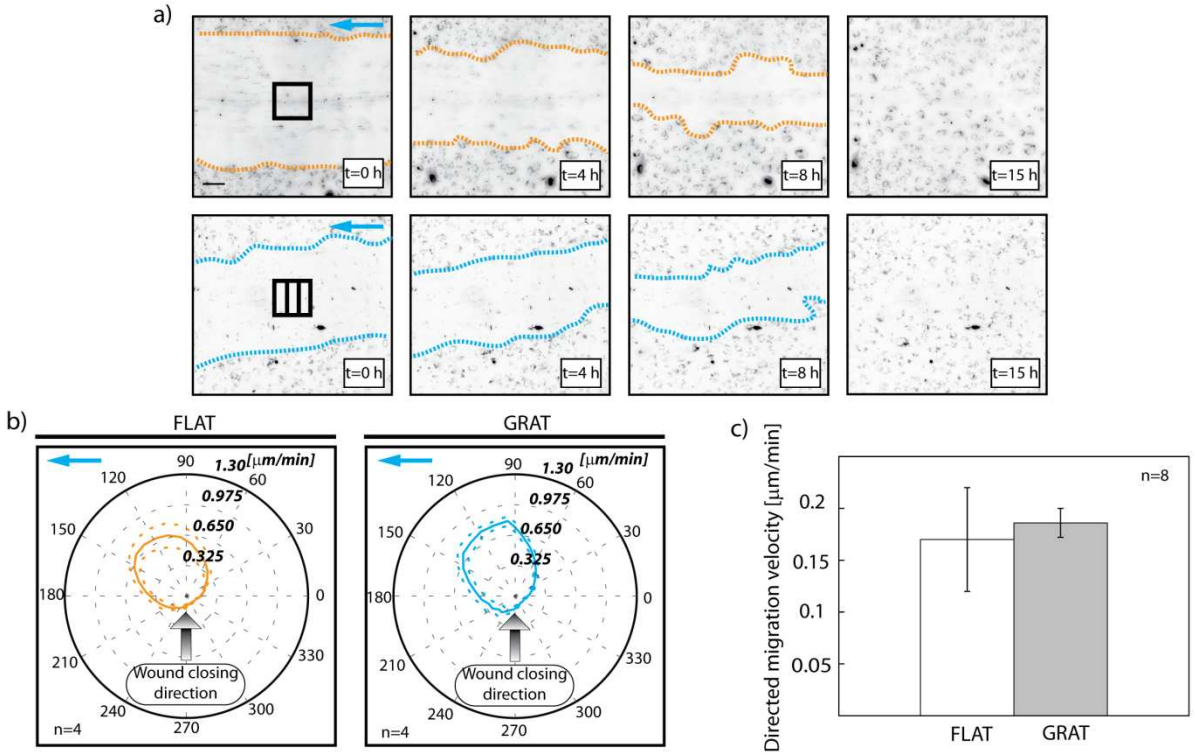

Supplementary Figure 4. Layer speed and directed migration velocity decrease over time on the flat substrate. The plots report the temporal evolution of the layer speed (a) and directed migration velocity (b) for the upstream and downstream edges on flat substrates (FLAT) and grating (GRAT). Reported values are time averages taken over 6 consecutive frames (120 min) overlapping by 45 min. The first temporal bin is located at 37.5 min spanning the interval [0,75] min. The number of analyzed time-lapse is reported in the upper right corner. Error bars represent the measured standard error of the mean.

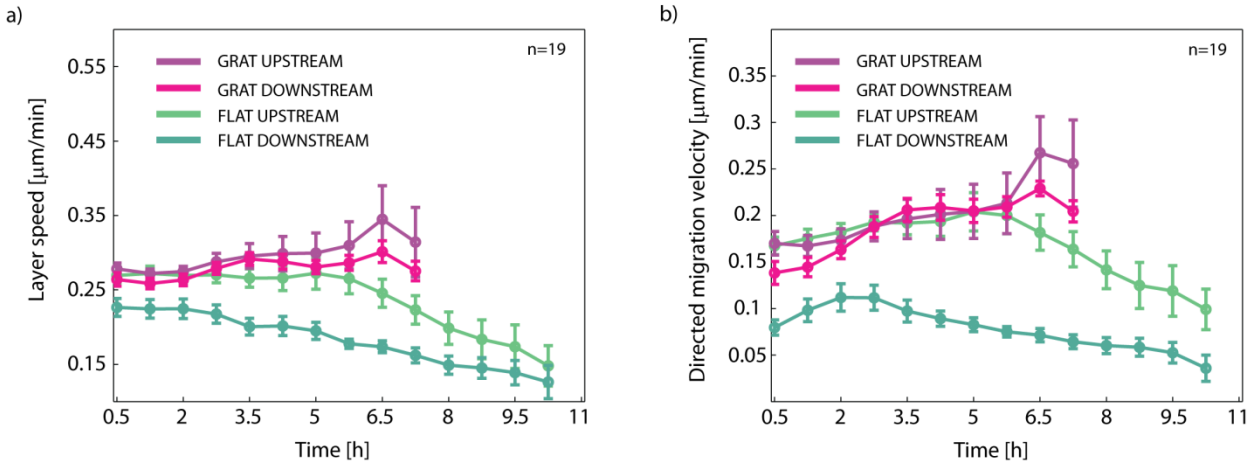

Supplementary Movie 1: Inverted fluorescent time-lapse of HUVEC wound healing on (**a**) gratings (GRAT; upper panel) and (**b**) flat substrate (FLAT; lower panel). For both configurations, constant flow (WSS of 1.4 Pa) was applied to the cell monolayer throughout the entire experiment (left to right; black arrow in the upper right corner). The gratings are orientated perpendicular to the wound. The time is reported in the upper left corner.

Supplementary Movie 2: Inverted fluorescent time-lapse of HUVEC wound healing on flat substrate. The movie provides a zoomed view of the upstream wound edge where border cells enter individually the open space. A constant flow (WSS of 1.4 Pa) was applied to the cell monolayer throughout the entire experiment (left to right). The time is reported in the upper left corner.